Phagocytosis-dependent ketogenesis in retinal pigment epithelium

Received for publication, December 1, 2016, and in revised form, March 13, 2017 Published, Papers in Press, March 16, 2017, DOI 10.1074/jbc.M116.770784

Juan Reyes-Reveles[‡], Anuradha Dhingra[‡], Desiree Alexander[‡], Alvina Bragin[‡], Nancy J. Philp[§1], and Kathleen Boesze-Battaglia[‡2]

From the [‡]Department of Biochemistry, School of Dental Medicine (SDM), University of Pennsylvania, Philadelphia, Pennsylvania 19104 and the [§]Department of Pathology, Anatomy and Cell Biology, Thomas Jefferson University, Philadelphia, Pennsylvania 19146

Edited by Dennis R. Voelker

Daily, the retinal pigment epithelium (RPE) ingests a bolus of lipid and protein in the form of phagocytized photoreceptor outer segments (OS). The RPE, like the liver, expresses enzymes required for fatty acid oxidation and ketogenesis. This suggests that these pathways play a role in the disposal of lipids from ingested OS, as well as providing a mechanism for recycling metabolic intermediates back to the outer retina. In this study, we examined whether OS phagocytosis was linked to ketogenesis. We found increased levels of β-hydroxybutyrate (β-HB) in the apical medium following ingestion of OS by human fetal RPE and ARPE19 cells cultured on Transwell inserts. No increase in ketogenesis was observed following ingestion of oxidized OS or latex beads. Our studies further defined the connection between OS phagocytosis and ketogenesis in wild-type mice and mice with defects in phagosome maturation using a mouse RPE explant model. In explant studies, the levels of β-HB released were temporally correlated with OS phagocytic burst after light onset. In the *Mreg*$^{-/-}$ mouse where phagosome maturation is delayed, there was a temporal shift in the release of β-HB. An even more pronounced shift in maximal β-HB production was observed in the *Abca4*$^{-/-}$ RPE, in which loss of the ATP-binding cassette A4 transporter results in defective phagosome processing and accumulation of lipid debris. These studies suggest that FAO and ketogenesis are key to supporting the metabolism of the RPE and preventing the accumulation of lipids that lead to oxidative stress and mitochondrial dysfunction.

The retinal pigment epithelium (RPE)[3] forms the outer blood retinal barrier and plays a central role in maintaining metabolic homeostasis in the outer retina through transport of nutrients and waste products (1, 2). Glucose, the primary energy substrate utilized by the outer retina is transported to the outer retina by the RPE. The glucose transporter (GLUT1) is expressed in the basal and apical membrane of the RPE and facilitates transport of glucose from the choroid circulation into the outer retina. Additionally, the RPE supports photoreceptor activity and outer-segment (OS) renewal through the retinoid visual cycle and ingestion of shed photoreceptor outer segments (1). On a daily basis, photoreceptors shed ~10% of their lipid and protein-rich OS, for uptake and degradation by the RPE (3, 4). Individual RPE cells phagocytose numerous OS daily; in the central mouse retina, each RPE cell digests the contents of over 200 photoreceptor outer segment tips daily (5). These ingested OS provide a rich source of fatty acids (6–8) for the RPE, suggesting that fatty acid β-oxidation (FAO) could support the energy demands of the RPE, thus sparing glucose for the outer retina (9).

Mitochondrial FAO is a main source for energy production in skeletal muscle, as well as heart and kidney tubular epithelium even when glucose supplies are plentiful (10). The complex mix of saturated and highly unsaturated fatty acids, which make up 50% of ingested OS (by weight), provides the RPE with substrates for mitochondrial and peroxisomal FAO (6). Porcine RPE metabolize saturated fatty acids via β-oxidation (11), whereas human, monkey, and frog RPE incorporates OS-derived arachidonic acid (20:4) and docosahexaenoic acid (22:6) into triacylglycerols and phospholipids (8, 12–14). Our own *in vitro* studies have demonstrated that human RPE cells can use palmitate (16:0), a major lipid component of OS for FAO (15). Use of these nutrients as metabolic substrates requires enzymes essential for FAO, including carnitine palmitoyl transferase 1A and the trifunctional protein complex, both of which are expressed in mouse and human RPE (16). Deficiencies in the long-chain 3-hydroxyl-CoA-dehydrogenase activity of the trifunctional protein leads to progressive pigment retinopathy, characterized by lipid accumulation, RPE atrophy, and pigment deposits (17). Similarly, lipid accumulation is found in the liver and kidney when FAO is slowed because of mutations or metabolic reprogramming and is often associated with fibrosis (18). We predict that in the RPE, mitochondrial dysfunction would not only lead to metabolic reprograming but would also disrupt the normal flow of nutrients to the outer retina.

This work was supported in whole or in part by National Institutes of Health Grants EY010420 (to K. B.-B.), EY 012042 (to N. J. P.), and EY026525 (to K. B.-B. and N. J. P.). The authors declare that they have no conflicts of interest with the contents of this article. The content is solely the responsibility of the authors and does not necessarily represent the official views of the National Institutes of Health.

[1] To whom correspondence may be addressed: Dept. of Pathology, Anatomy, and Cell Biology, Thomas Jefferson University, Philadelphia, PA 19146. Tel.: 215-503-7854; E-mail: nancy.philp@jefferson.edu.

[2] To whom correspondence may be addressed: Dept. of Biochemistry, SDM, University of Pennsylvania, Philadelphia, PA 19104. Tel.: 215-898-9167; E-mail: battagli@upenn.edu.

[3] The abbreviations used are: RPE, retinal pigment epithelium; OS, outer segments; β-HB, β-hydroxybutyrate; FAO, fatty acid oxidation; DHA, docosahexaenoic acid; ABC, ATP-binding cassette; HMGCS, 3-hydroxy-3-methylglutaryl-CoA synthase; hfRPE, human fetal RPE; MREG, melanoregulin.

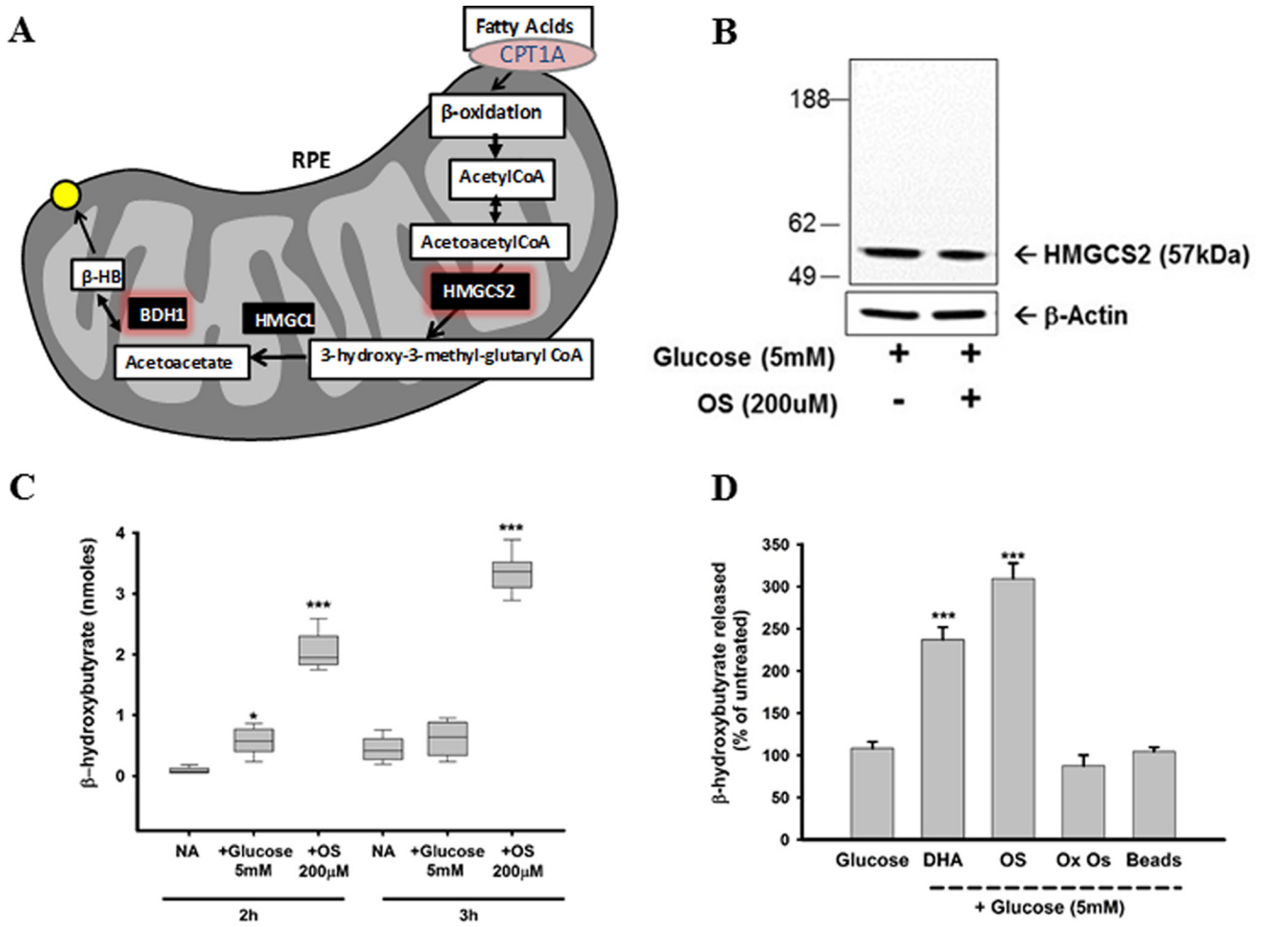

Figure 1. hfRPE generates β-HB through FAO of lipids from ingested outer segments. *A*, schematic representation of enzymatic reactions in ketogenesis. *B*, hfRPE expresses HMGCS2. *C*, β-HB is preferentially transported across the apical membrane of hfRPE after OS ingestion. hfRPE cells were incubated in apical chamber with glucose, OSs, or both, and the apical media were evaluated for β-HB content using a StanBio β-HB kit. *, $p < 0.05$; ***, $p < 0.001$., not significant. Plots are box-whisker plots showing median, with maximum and minimum range of the data for three independent experiments each done in triplicate. *D*, DHA serves as a substrate for FAO and ketogenesis, whereas oxidized OS and latex beads do not. hfRPE cells were incubated with glucose in the presence or absence of 200 μM DHA, 200 μM OS, 200 μM OxOS, or latex beads in apical chamber, and β-HB released was measured in the apical compartment using a StanBio β-HB kit. ***, $p < 0.001$. The values are means ± S.E. for three independent experiments, each done in triplicate.

A fate of mitochondrial acetyl-CoA derived from FAO is the formation of ketone bodies: acetoacetate and β-hydroxybutyrate (β-HB). The liver synthesizes ketones during fasting and lactation, providing a source of energy for peripheral tissues (19). Recently, we reported that the RPE expresses 3-hydroxy-3-methylglutaryl-CoA synthase 2 (HMGCS2), the rate-limiting mitochondrial enzyme required for ketogenesis. We showed *in vitro* that the RPE can generate β-HB from palmitate, a saturated fatty acid that makes up 15% of all lipids in the OS (6, 15). In the current study we tested the hypothesis that ingested OS serve as a substrate for RPE ketogenesis. Ketone body release was found to depend on diurnal phagocytosis of OS with defects in phagosome maturation contributing to metabolic delay as demonstrated in our mouse RPE explant models.

Results

Human RPE cells can utilize photoreceptor outer segments for ketogenesis

The RPE has a daily diet of fatty acid rich OS that could provide substrates for FAO and ketogenesis. HMGCS2, the rate-limiting mitochondrial enzyme in ketogenesis, converts acetoacetyl-CoA to 3-hydroxy-3-methyl-glutaryl-CoA as illustrated in Fig. 1*A*. HMGCS2 protein was expressed in polarized hfRPE cells (Fig. 1*B*). To determine whether human fetal RPE (hfRPE) uses lipids from OS as substrates for FAO and ketogenesis, polarized hfRPE in culture were fed purified OS, and β-HB released into the apical and basal media was quantified. The cells were incubated with Ringer's containing: 1) no substrate; 2) glucose (5 mM); 3) purified OS (200 μM, total phospholipid); or 4) glucose (5 mM) and purified OS (200 μM). β-HB levels in the apical and basal chambers were determined after 2- and 3-h incubations. As shown in Fig. 1*C*, hfRPE fed glucose alone produced little β-HB (0.83 ± 0.10 nmol in 3 h), whereas cells fed OS in the presence of 5 mM glucose released significantly more β-HB into the apical chamber (3.48 ± 0.11 nmol in 3 h). β-HB released with glucose + OS was time-dependent with an increase from 2.27 ± 0.03 nmol in 2 h to 3.48 ± 0.11 nmol in 3 h (Fig. 1*C*). β-HB levels in the basal chamber were below the limit of detection as reported previously with palmitate as the substrate for β-oxidation (15).

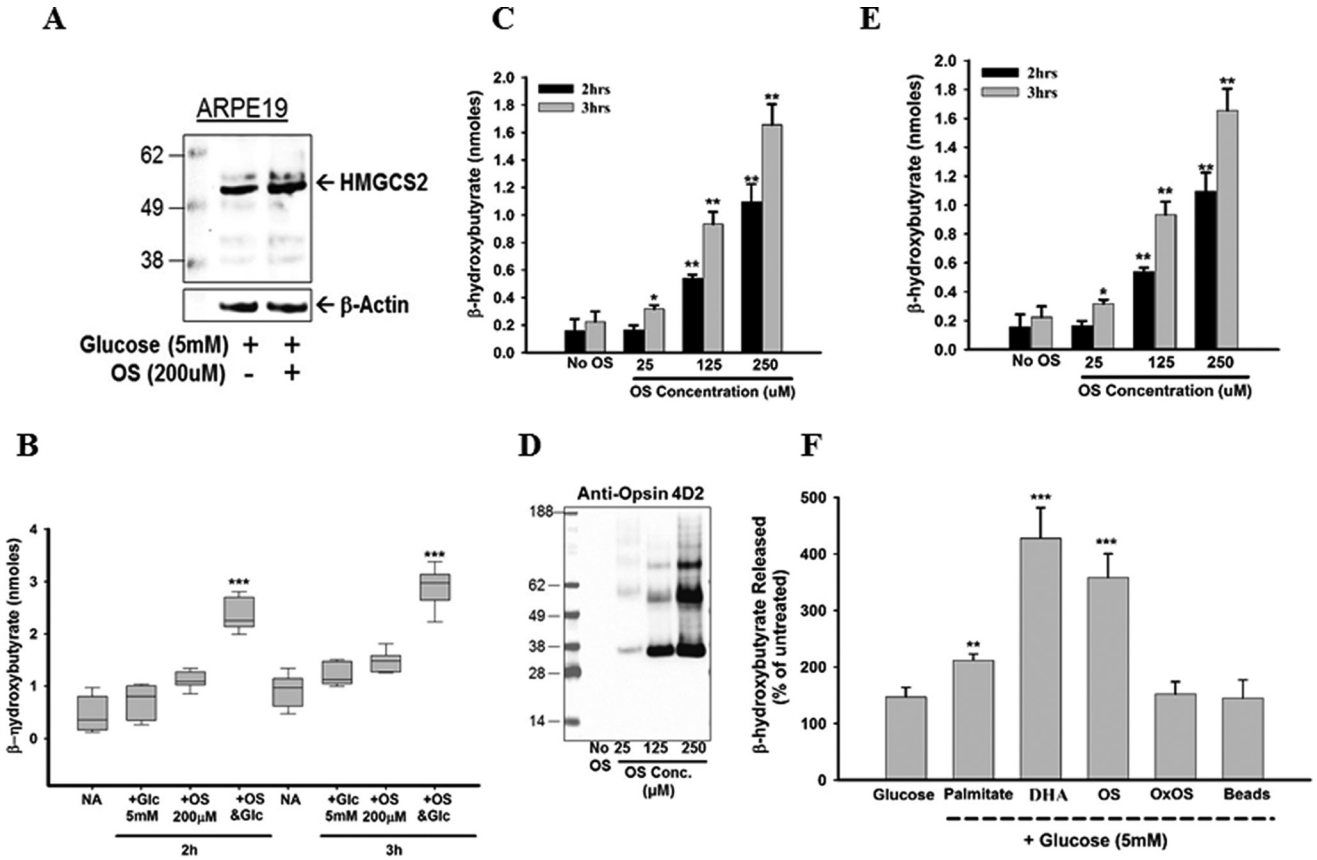

Figure 2. Generation of β-HB by ARPE19 cells is OS dose-dependent. *A*, ARPE19 cells express HMGCS2. *B*, β-HB is preferentially transported across the apical membrane of ARPE19 cells after OS ingestion. ARPE19 cells were incubated in apical chamber with glucose (*Glc*), OS, or OS plus glucose, and the apical supernatant was evaluated for β-HB content. **, $p < 0.005$. Plots are box-whisker plots showing median, with maximum and minimum range of the data for three independent experiments each done in triplicate. *C*, β-HB release increases as ingested OS levels increase. ARPE19 cells were incubated with glucose and increasing concentration of OSs (25–250 μM) in apical chamber for 3 h, and β-HB, the apical supernatant, was measured. *, $p < 0.05$; **, $p < 0.005$. The values are means ± S.E. for three independent experiments each done in triplicate. *D*, levels of opsin in ARPE19 cells challenged with increasing concentrations of OSs. Cleared ARPE19 cell lysates were prepared 3 h after OS challenge at the indicated concentrations and levels of opsin detected using anti-opsin 4D2 by immunoblot. *E*, ARPE19 cells were incubated with glucose and increasing concentration of OS-derived lipid liposomes in apical chamber for 3 h (25–200 μM), and then β-HB was measured in the apical compartment. **, statistical significance with p value < 0.005. The values are means ± S.E. for three independent experiments each done in triplicate. *F*, DHA serves as a substrate for FAO and ketogenesis, whereas oxidized OS and latex beads are not substrates. ARPE19 cells were incubated with glucose in the presence or absence of 200 μM DHA, 200 μM OS, 200 μM OxOS, or latex beads in the apical chamber, and β-HB was measured in the apical compartment content using a StanBio β-HB kit. ***, $p < 0.001$. The values are means ± S.E. for three independent experiments each done in triplicate.

The lipid composition of mammalian OS is unique with a relatively high concentration of DHA (7, 20, 21). When hfRPE cells were incubated with DHA conjugated to BSA (200 μM DHA + 5 mM glucose), a 237 ± 14.7% increase in β-HB secretion was observed as compared with Ringer's solution alone (Fig. 1*D*). To provide further evidence that the ingested OS lipids provided substrate for FAO and β-HB generation, OS were photo-oxidized under UV light. Oxidized fatty acids do not serve as substrates for FAO and β-HB generation; instead they are detoxified via a glutathione peroxidase (22). There was no increase in β-HB levels when hfRPE were incubated with photo-oxidized OS (oxOS) (Fig. 1*D*). Furthermore, latex beads were used as a control to determine whether non-lipid-containing phagocytosed particles provide a substrate for β-HB production. There was no increase in β-HB levels when hfRPE were incubated with latex beads (Fig. 1*D*).

The human RPE cell line, ARPE-19, expressed HMGCS2 (Fig. 2*A*) and released similar amounts of β-HB into the apical medium (3.10 ± 0.04 nmol) as hfRPE upon OS challenge in 5 mM glucose for 3 h (Fig. 2*B*). Little β-HB was released when OS were added in the absence of glucose. β-HB secretion was dose-dependent; as the concentration of ingested OSs increased from 25 to 250 μM, β-HB secretion increased 13-fold from 0.22 ± 0.08 to 1.66 ± 0.15 nmol (Fig. 2*C*). This dose-dependent increase in β-HB mirrored the extent of OS phagocytosed as reflected in the levels of rhodopsin in the RPE after 3 h (Fig. 2*D*). Moreover, 3 h after OS addition, the free-fatty-acid content of the RPE more than doubled from 10.3 ± 1.92 to 25.5 ± 1.13 μM. When only purified OS lipids in the form of liposomes were provided as substrates, there was a dose-dependent increase in β-HB released up to ~200 μM total phospholipid (Fig. 2*E*). Similar levels of β-HB were released into the apical chamber with OS and purified lipids, suggesting that protein-derived metabolic intermediates were not the source of ketones. Analogous to hfRPE, no increase in β-HB was detected when ARPE19 was incubated with oxOS or latex beads (Fig. 2*F*). DHA was also a substrate for ketogenesis in ARPE19.

Melanoregulin (MREG) is an intracellular cargo-sorting protein required for the degradation of OS disks (21, 22). It is a LC3-binding partner that is critical for complete degradation of

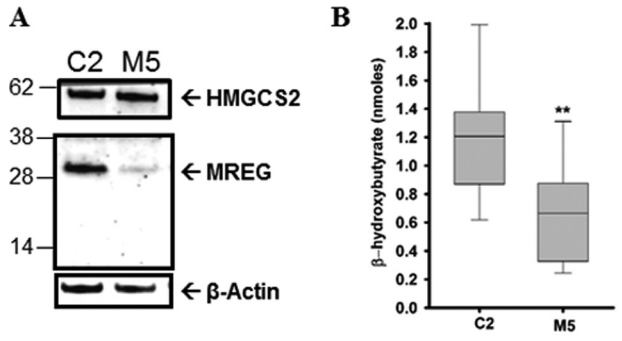

Figure 3. Defective phagosome maturation contributes to diminished apical β-HB. *A*, Western blot analysis of ARPE-19 cell lysates from cells stably transfected with control shRNA (C2) or MREG ShRNA (M5) both C2 and M5 cells have similar HMGCS2 levels. *B*, C2 and M5 ARPE-19 cells were incubated with glucose (5 mM) and OSs (200 μM) in the apical chamber for 3 h, and β-HB was measured in the apical compartment. Box-whisker plot representing the median and for three independent experiments each done in triplicate, with maximum and minimum range of the data. **, $p < 0.005$ compared with C2, with Student's *t* test.

OS through LC3-associated phagocytosis (35). To determine whether delayed phagosome degradation correlated with diminished β-HB secretion, MREG-deficient ARPE19 cells (MREG KD, designated M5) were fed OS (Fig. 3). In M5 cells, β-HB release decreased by ~50% at the 3-h time point (Fig. 3*B*). This decrease was not due to diminished OS uptake because loss of MREG did not affect OS uptake *in vitro* or *in vivo* (23, 24). Moreover, the HMGCS2 enzyme levels in the *MREG* KD (M5) were comparable with controls (C2) (Fig. 3*B*).

BHB production is temporally correlated with outer segment shedding and phagocytosis

In the mouse retina, *Hmgcs2* was detected in RPE but was not detected in the neural retina as determined by *in situ* hybridization with an *Hmgcs2*-specific probe (Fig. 4*A*). The HMGCS2 protein was expressed in mouse RPE where it co-localized with the mitochondrial enzyme COXIV (Fig. 4*B*). To determine whether *in vivo* ketogenesis is linked to FAO of ingested OS lipids, we developed an *ex vivo* assay. Eyes were isolated at different times in the light-dark cycle, and β-HB release was measured from mouse RPE explants as illustrated schematically in Fig. 4*C*. The number of phagosomes in mouse RPE peaks within an hour after light onset (Refs. 25 and 26 and Fig. 5*A*). We reasoned that if RPE cells utilize ingested OS as substrate for ketogenesis, β-HB production should increase following ingestion and degradation of outer segments. Therefore, we measured the release of β-HB from isolated RPE choroid explants isolated at different times after light onset. In these experiments, posterior eyecups were prepared and immediately incubated in Ringer's solution as detailed previously (15). The amount of β-HB released was measured 2 h after explant harvest. As shown in Fig. 4*D*, the highest levels of β-HB were correlated with RPE harvest at 7 a.m. (lights on), a point at which the RPE generally ingests the largest percentage of OS; β-HB levels subsequently decreased with no other statistically significant changes. HMGCS2 levels were highest at 7 a.m. harvest time (9 a.m. assay time), with no significant change in RPE HMGCS2 levels over the remaining 12-h time analyzed.

The peak time of β-HB production is shifted in mutant mice that exhibit delayed degradation of ingested outer segments

To demonstrate a temporal link between phagosome degradation and ketogenesis, we analyzed a mouse model of dysfunctional phagosome maturation: the $Mreg^{-/-}$ mouse. The $Mreg^{-/-}$ mouse exhibits a phagocytic burst at light onset; however, phagosome levels remain elevated for up to 8 h when compared with control C57Bl6/J RPE (Fig. 5*A*). HMGCs2 was expressed in $Mreg^{-/-}$ RPE mitochondria (Fig. 5*B*) with protein levels following a time-dependent distribution profile similar to that observed in wild-type C57Bl6/J mice (Fig. 5*C*), with a peak at 7 a.m. harvest time (9 a.m. assay time). β-HB release, however, did not follow the same temporal profile as seen in wild-type mice; delayed phagosome maturation resulted in a shift in peak time of β-HB production from 7 a.m. harvest and 9 a.m. assay to 10 a.m. harvest time corresponding to 12 p.m. assay time (Fig. 5*D*). This was a 3-h delay in maximal β-HB released. An even more pronounced shift in maximal β-HB production was observed in the $Abca4^{-/-}$, in which loss of the ABCA4 transmembrane transporter (27) results in defective phagosome processing and accumulation of lipid debris (28). Maximal β-HB release in the $Abca4^{-/-}$ was observed 6 h after light onset (Table 1). In addition to a temporal shift in the maximal release of β-HB, the amount of β-HB released was less in the $Abca4^{-/-}$, than control C57Bl6/J (Table 1). Collectively, these results suggest that phagosome maturation and processing by the RPE are integral to ketogenesis and transport of β-HB to the outer retina.

Discussion

The participation of the RPE in photoreceptor renewal has been known for almost 50 years. Bok and Young (3, 4) showed that the RPE was involved in the disposal phase of shed OS. In their 1969 paper, they noted that further work was needed to understand how the phagocytized OS material was "destroyed" (4). We propose that the daily fat intake of the RPE through OS ingestion is similar to the lipid load of the hepatocyte. Individuals consuming a standard Western diet metabolize ~100 g of fat daily or 0.4 nmol of fatty acids, with individual hepatocytes responsible for the metabolism of 0.1 pmol of fatty acid per day. Human RPE cells ingest and process 30 OS daily, which is equivalent to 0.1–0.15 pmol of fatty acid per cell (5). Herein we present the novel observation that the phagocytic function of the RPE provides metabolic substrates for RPE FAO and ketogenesis. These processes allow the RPE to spare glucose for the outer retina and prevents the accumulation of lipid debris (9).

Our previous studies demonstrated that hfRPE utilize the 16-carbon fatty acid, palmitate as a substrate for FAO and ketogenesis (15). Herein we extended those studies to show that after ingestion of OS, the RPE produces β-HB. The relationship between OS degradation and the apical release of β-HB was firmly established in our *in vitro* models: hfRPE and ARPE19. Dysregulated phagosome processing, which occurs in the Mreg-KD M5 ARPE19 cells, resulted in decreased β-HB released. Given that OS uptake is not reduced in the Mreg-KD, the decreased β-HB is likely due to the delay in phagosome maturation documented in these cells (23). Collectively, our *in*

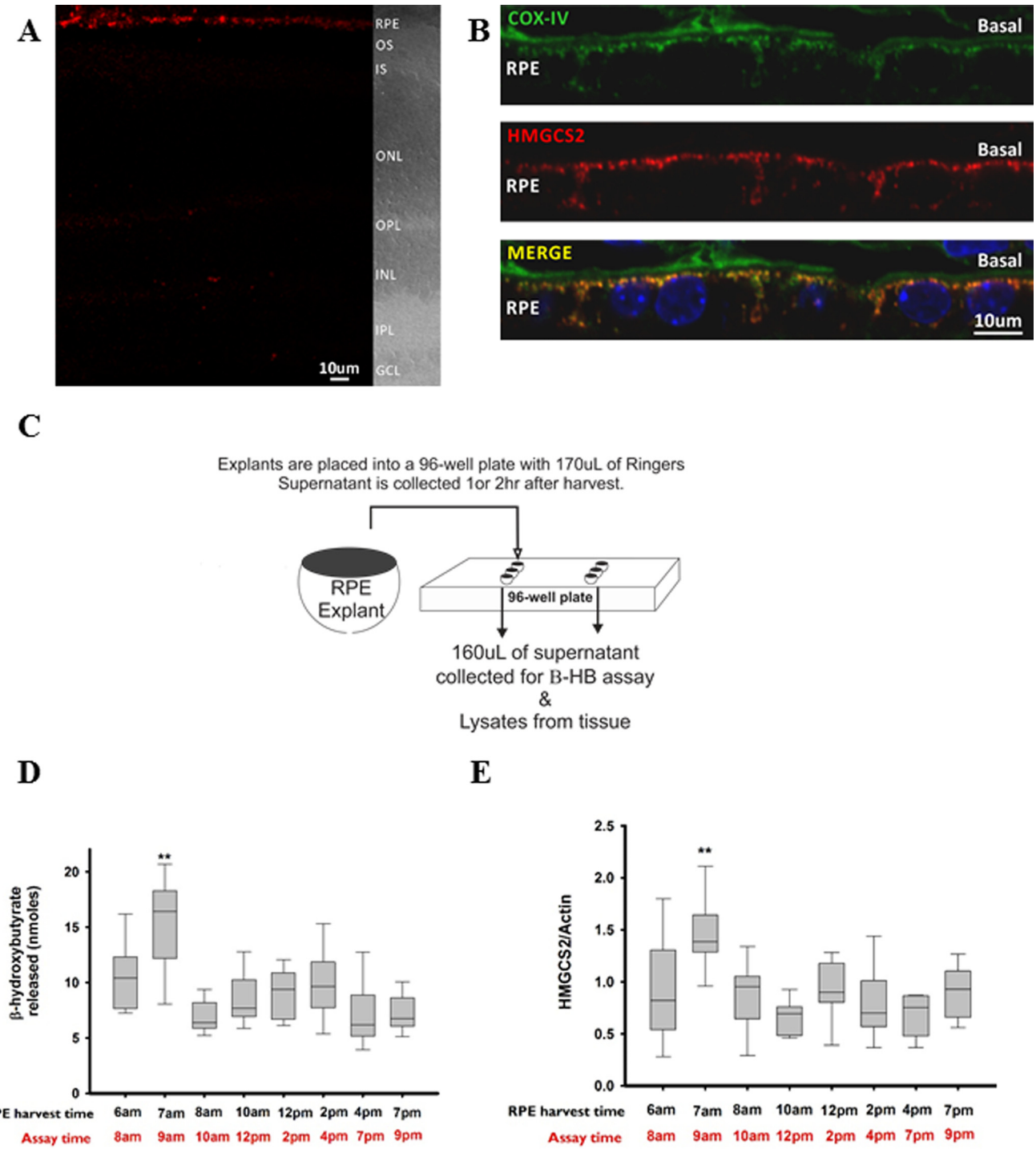

Figure 4. β-HB secretion from mouse RPE correlates with time of day. *A*, *Hmgcs2* is preferentially expressed in the RPE. *In situ* hybridization with an Hmgcs2 specific probe (in *red*) using RNAscope. Confocal micrograph of albino retinal section stained for HMGCS2 probe using RNAscope technology (*left*) and transmitted light image to show the retinal layers (*right*). HMGCS2 transcript is highly restricted (*red puncta*) to the RPE. *IS*, inner segments; *ONL*, outer nuclear layer; *OPL*, outer plexiform layer; *INL*, inner nuclear layer; *IPL*, inner plexiform layer; *GCL*, ganglion cell layer. *B*, localization of HMGCS2 to mitochondria in mouse RPE. Confocal micrograph of wild-type C57Bl6/J retinal sections immunostained for COXIV (*green*) and HMGCS2 (*red*) shows exclusively mitochondrial localization of HMGCS2 in the RPE. Nuclei are indicated in the merged image as *blue*. As expected, most of the staining is in the basolateral RPE. *C*, schematic representation of experimental design and RPE/choroid explant isolation. *D*, β-HB is released from mouse RPE/choroid explants upon OS ingestion. Supernatant was collected from RPE/choroid explants harvested as shown in *C*, and β-HB levels were determined immediately. *, $p < 0.05$; **, $p < 0.005$. Plots are box-whisker plots showing median, with maximum and minimum range of the data from six individual mice at each time point. *E*, HMGCS2 protein levels normalized to actin in RPE explants utilized for β-HB release experiments in *D*. Cleared lysates were isolated immediately after the 2-h sample was collected, and Western blotting for HMGCS2 was performed as described under "Experimental procedures." **, $p < 0.005$. Plots are box-whisker plots showing median, with maximum and minimum range of the data for 12 eyes from 6 individual mice at each time point.

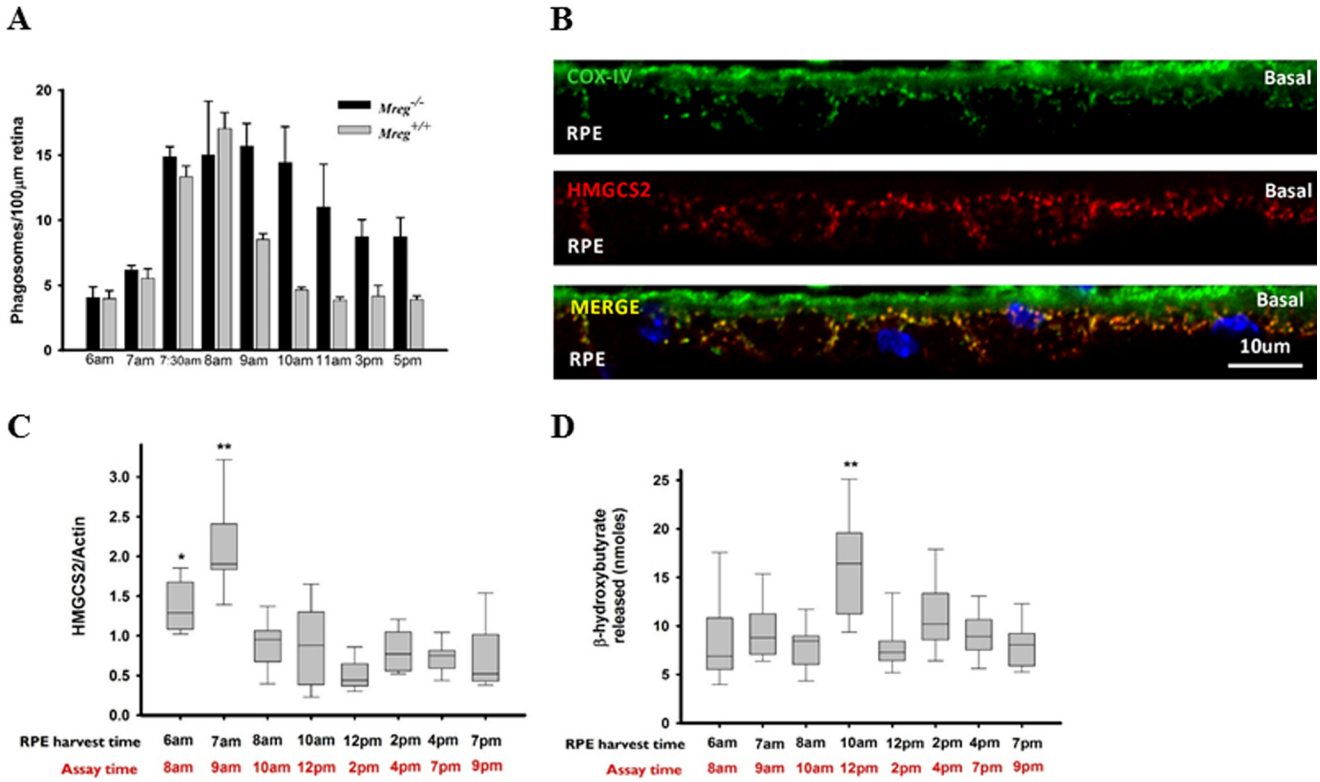

Figure 5. β-HB secretion is delayed coincident with slowed phagosome maturation in mouse RPE. *A*, loss of MREG leads to phagosome accumulation in the RPE. Phagosome numbers per 100 μm of RPE length in $Mreg^{+/+}$ and $Mreg^{-/-}$ mice at different time points relative to lights on. Counts were done in duplicate on 10 individual areas per mouse in a total of 2 mice/4 eyes with analyst blind to the strain of mouse. The results are means ± S.E. *B*, localization of HMGCS2 to mitochondria in mouse $Mreg^{-/-}$ RPE. Confocal micrographs of $MREG^{-/-}$ retinal sections immunostained for COXIV (*green*) and HMGCS2 (*red*) showing mitochondrial localization of HMGCS2 similar to WT. Nuclei are indicated in the merged image as *blue*. Note that the basolateral pattern of mitochondrial distribution closely resembling the WT. *C*, HMGCS2 protein levels in RPE explants utilized for β-HB release experiments in *D*. Cleared lysates were isolated immediately after the 2-h sample was collected, and Western blotting for HMGCS2 was performed as described under "Experimental procedures." **, $p < 0.005$. Plots are box-whisker plots showing median, with maximum and minimum range of the data for 12 eyes from 6 individual mice at each time point. *D*, β-HB is released from mouse RPE/choroid explants upon OS ingestion. Supernatant was collected from RPE/choroid explants, and β-HB levels were determined immediately. *, $p < 0.05$; **, $p < 0.005$. the plots are box-whisker plots showing median, with maximum and minimum range of the data for 12 eyes from 6 individual mice at each time point.

Table 1

Peak of maximal β-HB release varies with phagosome degradation efficiency

The table shows a comparison of the time after light onset when the maximal amount of β-HB was detected in the media. The values are the means ± S.E. of 12 eyes from 6 individual mice at each time point.

Strain	Peak of β-HB release (time after light onset)	β-HB in media
	h	μM
C57Bl6/J	2	15.0 ± 1.89
$Mreg^{-/-}$	5	13.3 ± 0.94
$Abca4^{-/-}$	6	9.52 ± 2.04[a]

[a] Statistical significance with p value < 0.050.

vitro studies show that human RPEs express HMGCS2, the rate-limiting enzyme in ketogenesis, and generate β-HB upon OS digestion. These studies are the first to link ketogenesis with phagosome maturation in the RPE. Furthermore, DHA, like ingested OS, provides substrate for ketogenesis, whereas photo-oxidized OS does not. These findings are consistent with our hypothesis that FAO plays an important role in facilitating the disposal of ingested OS, suggesting that FAO may be the primary pathway used by the RPE for energy production. Our previous studies suggest that RPE cells used ≈50% of acetyl-CoA derived from palmitate to produce β-HB (15). In these studies, feeding hfRPE cells 200 μM total phospholipid equivalent to ≈100 nmol of fatty acid substrate resulted in the release of 15 nmol of β-HB into the apical medium.

The glucose requirement in the cultured model system Fig. 2*B* is likely 2-fold, glucose is required for phagosome maturation and is likely the source of reducing equivalents. In differentiated RPE, as is the case here, analysis of a panel of metabolites demonstrated that RPE cells produce NADH more rapidly from glucose than oxidative substrates (38). The glucose requirement is likely important *in vivo* as the relationship between fatty acids and inhibition of glucose utilization is regulated by the Randle cycle (9).

OS contain a prodigious amount of long-chain fatty acids (species with 20+ carbons); therefore, their oxidation relies on peroxisomal degradation (29). These longer chain fatty acids are converted to acyl carnitine derivatives in the peroxisome, which can be oxidized by the mitochondria. Our observation that RPE can generate β-HB from DHA, a 22-carbon unsaturated fatty acid, suggests that in addition to detoxification, peroxisomes play an essential role in maintaining lipid homeostasis.

Ex vivo studies with RPE explants showed that β-HB production was linked to the shedding/phagocytosis phase of photoreceptor renewal. RPE/choroid harvested at different times after the onset of light showed a peak of β-HB release when

isolated from mice at 7 a.m., when the burst of shedding and phagocytosis occurs. This peak is coincident with the maximal levels of HMGCS2. Consistent with our findings, it was recently reported the levels of β-HB increase in the outer retina after light onset (30).

The link between β-HB production and phagosome maturation is demonstrated in our studies on $Mreg^{-/-}$ mouse RPE explants, where phagosome maturation is delayed. In explants from the $Mreg^{-/-}$ mouse, the peak time of β-HB released was shifted to 12 p.m., 5 h after light onset. The peak of HMGCS2 expression was identical to that observed in WT (C57Bl6/J), at 7 a.m. At this time point, the $Mreg^{-/-}$ RPE explant released 9.83 ± 1.30 nmol of β-HB compared with 15.03 ± 1.89 nmol in the WT RPE explant. These findings suggest that the increase in HMGCS2 is regulated by signaling pathways downstream of ingestion, and substrate availability determines β-HB generation. Mutations in the photoreceptor-specific flippase ABCA4 lead to accumulation of the toxic bisretinoid A2E, resulting in atrophy of the RPE and death of the photoreceptor cells (28, 36). Many blinding diseases are associated with these mutations including Stargardt's disease (STGD1), cone-rod dystrophy, retinitis pigmentosa, and increased susceptibility to age-related macular degeneration. A characteristic of this model is an increase in oxidized lipid and alkalinization of lysosomes, thus rendering them less able to degrade ingested OS (31). Our explant studies (Table 1) show not only a delay in β-HB released but also a decrease in total β-HB released over the 12-h time frame studied. These results, coupled with our *in vitro* observations, support the hypothesis that FAO and ketone body formation prevent the accumulation of lipid in the RPE.

We propose that providing the RPE with a daily bolus of lipid rich OS shifts their metabolism to fatty acid rather than glucose oxidation. RPE FAO would thus spare glucose for the outer retina, consistent with studies establishing that glucose is required to support the health of rod and cone photoreceptor cells (32). Support for the notion that RPE spares glucose for the outer retina comes from recent studies characterizing the distribution fluorescent 2-deoxy glucose in retinas of mice with P23H mutation in rhodopsin that results in a loss of photoreceptor cells. In these studies, fluorescent glucose was transported into the retina in wild-type mice, whereas in the P23H mice it was "sequestered" in the RPE. Sequestration of glucose in RPE resulted in nutrient deprivation to cones, causing them to lose their outer segments and eventually their connecting cilium (32). Based on our model of metabolic coupling in the outer retina, we predict that sequestration of glucose in the RPE was due to metabolic reprogramming of the RPE. In the absence of a supply of fatty acids from rod outer segment renewal, the RPE utilized glucose as an energy substrate.

Mitochondrial dysfunction and a shift from oxidative to glycolytic metabolism are found in several age-related diseases including age-related macular degeneration (33). In the RPE-specific VHL-KO mouse, in which HIFs are stabilized, an increase in glycolytic and a decrease in genes associated with FAO and ketogenesis, including HMGCS2 was observed (34). A decrease in HMGCS2 would be expected to reduced fatty acid oxidation and an increase in lipid debris in the RPE and subretinal space. Consistent with this hypothesis, an increase in lipid debris in the RPE and a thickening of Bruch's membrane was observed in the RPE-specific VHL-KO mouse (34).

In addition to mitochondrial dysfunction, changes in phagosome maturation also lead to lipid accumulation. In this regard, Jiang *et al.* (35), show that dysregulated phagosome trafficking as observed in the absence of kinesin-1 light chain 1 leads to excessive accumulation of RPE and sub-RPE deposits. Our studies herein now provide a working hypothesis by which to understand the molecular mechanism of lipid accumulation. They suggest that FAO and ketone body formation is necessary to prevent lipid accumulation in RPE subretinal space. Therefore, stimulation of FAO should provide a means by which to increase fatty acid utilization providing a viable therapeutic for decreasing lipid accumulation.

Experimental procedures

Materials

Commercially available antibodies were acquired as follows: mouse anti-actin (A2228; Sigma-Aldrich), rabbit anti-HMGCS2 (ab137043, EPR8642; Abcam, Cambridge, MA), mouse anti-opsin mAb 4D2 (generous gift from Dr. R. Molday, University of British Colombia), goat anti-mouse and goat anti-rabbit HRP-conjugated secondary antibody (Thermo Fischer Scientific). For the lipids, palmitate was purchased from TCI America (catalog no. P0007; Portland, OR) and DHA from Tocris Bioscience (catalog no. 3687; Bristol, UK). Latex beads (F8811) were purchased from Life Technologies. For immunohistochemistry, we used rabbit anti-HMGCS2 antibody (ab137043; Abcam), mouse anti-CoxIV subunit 1 (1D6E1A8; Invitrogen), Alexa Fluor 594 donkey anti-mouse and Alexa Fluor 647 donkey anti-rabbit IgGs (Life Technologies), and Hoechst 33258 (Ana Spec Inc. Fremont, CA).

Animals

For immunostaining experiments, 11–12-month-old C57Bl6/J mice (obtained from the Jackson Laboratory) were used. $Mreg^{dsu}$ (a.k.a. $Mreg^{-/-}$) mice (11–12 months old) were obtained from Drs. Jenkins and Copeland (Methodist Hospital Research Institute) (36). We have used the $Mreg^{-/-}$ designation herein. Pigmented, $Abca4^{-/-}$ mice (129S4/SvJae-ABCA4tm1Ght, 11 months old) were provided by Dr. Gabriel Travis (David Geffen School of Medicine, University of California, Los Angeles, CA) (37). The mice were housed under standard cyclic light conditions: 12-h light/12-h dark and fed *ad libitum*, with both female and male mice used in these studies. All procedures involving animals were approved by the University of Pennsylvania Institutional Animal Care and Use Committee and were in accordance with the Association for Research in Vision and Ophthalmology guidelines for use of animals in research.

RPE explant harvest

C57Bl6/J, $Abca4^{-/-}$ or $Mreg^{-/-}$ mice were sacrificed at specific times relative to light onset (6 a.m., 7 a.m. (light onset), 8 a.m., 10 a.m., 12 p.m., 2 p.m., 4 p.m., and 7 p.m.) with at least three mice of each genotype analyzed at each time point. Both male and female 12–15-month-old mice were analyzed for all

strains tested. Extracted eyes were placed in ice-cold Ringer's solution. To isolate the RPE layer, the lens, optic nerve, excess muscle and fat, iris epithelium, and neural retina were removed under a dissection microscope, the RPE layer was exposed. For mice sacrificed at 6 a.m., 60 min before lights on, the removal of lens, optic nerve, and excess muscle and fat was done under dim red light. All procedures were performed on ice. RPE explants were placed in a 96-well plate with 170 μl of Ringer's solution and incubated at 37 °C, 5%CO_2. 1 or 2 h after harvest, 100 and 50 μl of Ringer's solution were collected for β-HB determination. RPE cell lysates were immediately prepared from the explants for immunoblotting.

Cell culture

hfRPE cells—T75 flasks of P0 hfRPE were obtained from the Drs. Sheldon Miller and Arvydas Maminishkis at the National Eye Institute of Health. hfRPE cells were trypsinized from a T25 flask and seeded onto 12-well Transwells at $\approx 1.25 \times 10^5$ cells/well (passage 1; P1) as previously described (38). The cells were used for experiments 3–4 weeks after plating when transepithelial resistance was greater than 500 $\Omega \cdot cm^2$) prior to experimentation. For dedifferentiated hfRPE, the cells were plated at 1.25×10^5 cells/well.

ARPE-19 cells—(CRL-2302, ATCC) were maintained as described (39, 40). The cells were grown on Transwell filters (12-well, 0.4-μm pore size) maintained in DMEM/F12 with 1% fetal bovine serum (Sigma) and 5% penicillin-streptomycin (Life Technologies, Inc.) at 37 °C, 5%CO_2. Individual filters were seeded with 1.6×10^5 cells/well in a total volume of 0.5 ml in the apical chamber and 1.5 ml of medium in the basal chamber with the medium changed twice weekly beginning the day after plating. Polarized MREG knockdown (M5) and Ctrl (C2) ARPE19 cells were cultured as described (24).

Immunoblotting—Cleared RPE and retinal lysates were prepared in radioimmune precipitation assay buffer with 1% protease inhibitor mixture (Sigma; P8340) and 2% phosphatase inhibitor mixture 2 (Sigma; P5726) (39). Lysates normalized for protein (10–15 μg) were separated on 4–12% Bis-Tris-PAGE (Invitrogen) under reducing conditions and transferred to PVDF membranes (Millipore, Billerica, MA). After transfer, membranes were blocked with 5% milk in PBS, 0.1% Tween 20 for 1 h at room temperature and incubated with primary antibodies for anti-HMGCS2 (1:1,000) as described (41), anti-β-actin (1:5,000), or anti-opsin (4D2) (1:1,000) overnight at 4 °C. Membranes were washed and incubated with goat anti-rabbit (1:3,000) or goat anti-mouse (1:3,000) horseradish peroxidase-conjugated secondary antibodies for 1 h at room temperature. The blots were developed using ECL (SuperSignal® West Dura extended duration substrate (Thermo Scientific) and captured on ImageQuant™ LAS 400 image reader (GE Healthcare) and quantified as described (42).

Immunohistochemistry—Immunostaining was performed on frozen sections of mouse retinas (43). Mice were anesthetized and perfused with 4% paraformaldehyde in PBS (pH 7.4). Eyes were enucleated, incised just below the lens, cryoprotected in 30% sucrose, and embedded in OCT. 7-μm cryosections were permeabilized and blocked in blocking solution containing 4% BSA and 0.2% Triton X-100 in PBS (PBST), incubated with rabbit anti-HMGCS2 antibody (ab137043; Abcam) and mouse anti-CoxIV (459600; Invitrogen) diluted in blocking solution (1:200) at 37 °C for 1 h, washed three times with PBST, incubated in donkey anti-rabbit and anti-mouse secondary antibodies conjugated to Alexa Fluor dyes (1:1,000) and Hoechst 33258 (1:10,000) at 37 °C for 1 h, and washed three times. For controls, the primary antibody step was eliminated. Sections were mounted in Cytoseal mounting medium (Electron Microscopy Sciences, Hatfield, PA). Images were captured on a Nikon A1R laser scanning confocal microscope with a PLAN APO VC 60× water (NA 1.2) objective at 18 °C, and the data were analyzed using Nikons Elements AR 4.30.01 software (39). In co-distribution analyzes, the Pearsons' coefficient was at least 0.55, and analysis included standard LUT adjustment.

In situ hybridization—HMGCS2 RNA *in situ* hybridization was performed using RNAscope 2.5 HD assay kit (Advanced Cell Diagnostics, Newark, CA) using mouse HMGCS2 probe (Mm Hmgcs2, catalog no. 437141; Advanced Cell Diagnostics). Briefly, fresh frozen sections from 3-month-old C57Bl6/J mouse retina were fixed in 4% prechilled paraformaldehyde at 4 °C for 15 min and dehydrated in ethanol series, followed by pretreatment, hybridization, amplification, and detection (red assay) steps as per the manufacturer's instructions. Images were captured with a 60× objective (NA 1.2) using Nikon A1R laser scanning confocal microscope.

Metabolic studies

Preparation of metabolic substrates—Ringer's solution was prepared using the basic chemical components of RPE cell culture medium: $CaCl_2$ (1.1 mM), KCl (4.2 mM), NaCl (120.6 mM), $NaHCO_3$ (14.3 mM), $MgCl_2$ (0.3 mM), and HEPES (15 mM). HEPES was dissolved separately and titrated to pH 7.4 with *N*-methyl-D-glucamine. L-Carnitine (1 mM) in Ringer's solution was added before each experiment; the solution was equilibrated to pH 7.4 with CO_2 and filter-sterilized. The BSA-vehicle control and BSA-conjugated palmitate and docosahexaenoic acid substrates were prepared exactly as described previously (38). Photoreceptor OSs purified from frozen dark-adapted bovine retinas (44) or purified outer segment liposomes (45) were added to cultured RPE cells as indicated in the figure legends. The phospholipid content of the OS or OS liposomes was determined using a Malachite Green assay kit per the manufacturer's instructions (K-1500; Echelon Biosciences) as originally described (46). OS were photo-oxidized by irradiation under UV light for 72 h as described (47).

On the day of experiment, the outer segments were thawed, pelleted, and resuspended in Ringer's solution at a final concentration of 200 μM (based on total phospholipid content). Latex beads were suspended in Ringer's solution and added at an multiplicity of infection equivalent to the calculated number of outer segments in 200 μM. The BSA-conjugated palmitate and DHA substrates were diluted from the frozen stocks to obtain a final working concentration of 200 μM, and 500 μl was added. 5 mM glucose was made fresh daily in water. All substrates were added in Ringer's solution alone or with the addition of 5 mM glucose as indicated in the figure legends.

β-Hydroxybutyrate assay—Ringer's solution containing different substrates was added to the apical chamber of ARPE-19

or hfRPE cells grown on 12-well Transwell filters. Ringer's solution (115 μl) was collected from the apical and basal chamber and analyzed for β-HB at the 2- and 3-h time points essentially as described (15). The β-HB levels were determined using the β-hydroxybutyrate LiquiColor kit (Stanbio, Boerne, TX; catalog no. 2440-058). In this assay, reagent A was mixed with reagent B at a 6:1 ratio, and 150 μl of this mixture was added to 100 μl of samples or β-HB standards in each well. The plate was light-protected and incubated at 37 °C for 1 h with gentle shaking before absorbance at 492 nm was measured. Free fatty acids were measured using a colorimetric enzymatic fatty acid quantification assay (ab65341; Abcam) as described (48). No β-HB was detected with OS alone.

Statistical analyses

Cell culture β-HB release measurements are presented as means ± S.E. with statistical significance determined using Student's t test with values compared with Ringer's solution alone. The explant studies are presented as means ± S.E. of β-HB released. The mouse explant data were analyzed using 1-way analysis of variance and Holm-Sidak post hoc test. *, $p < 0.05$; **, $p < 0.005$; ***, $p < 0.001$. Statistical analyses were all performed using Sigma plot version 12.3.

Author contributions—K. B.-B. and N. J. P. conceived and designed the experiments, coordinated the study, and wrote the paper. J. R.-R. contributed to experimental design, performed the experiments, and provided initial data analysis for Figs. 1–5. D. A., A. D., and A. B. provided technical assistance and contributed to the preparation of the figures. All authors reviewed the results and approved the final version of the manuscript.

Acknowledgments—We thank Dr. Gabriel Travis (UCLA) for the Abca4$^{-/-}$ mice and Dr. Robert Molday (University of British Columbia) for the anti-opsin mAb-4D2.

References

1. Strauss, O. (2005) The retinal pigment epithelium in visual function. *Physiol. Rev.* **85,** 845–881
2. Burke, J. M., and Hjelmeland, L. M. (2005) Mosaicism of the retinal pigment epithelium: seeing the small picture. *Mol. Interventions* **5,** 241–249
3. Young, R. W. (1967) The renewal of photoreceptor cell outer segments. *J. Cell Biol.* **33,** 61–72
4. Young, R. W., and Bok, D. (1969) Participation of the retinal pigment epithelium in the rod outer segment renewal process. *J. Cell Biol.* **42,** 392–403
5. Volland, S., Esteve-Rudd, J., Hoo, J., Yee, C., and Williams, D. S. (2015) A comparison of some organizational characteristics of the mouse central retina and the human macula. *PLoS One* **10,** e0125631
6. Fliesler, S. J., and Anderson, R. E. (1983) Chemistry and metabolism of lipids in the vertebrate retina. *Prog. Lipid Res.* **22,** 79–131
7. Bazan, N. G. (1989) The metabolism of omega-3 polyunsaturated fatty acids in the eye: the possible role of docosahexaenoic acid and docosanoids in retinal physiology and ocular pathology. *Prog. Clin. Biol. Res.* **312,** 95–112
8. Chen, H., and Anderson, R. E. (1993) Metabolism in frog retinal pigment epithelium of docosahexaenoic and arachidonic acids derived from rod outer segment membranes. *Exp. Eye Res.* **57,** 369–377
9. Randle, P. J. (1998) Regulatory interactions between lipids and carbohydrates: the glucose fatty acid cycle after 35 years. *Diabetes Metab. Rev.* **14,** 263–283
10. Houten, S. M., Violante, S., Ventura, F. V., and Wanders, R. J. (2016) The biochemistry and physiology of mitochondrial fatty acid β-oxidation and its genetic disorders. *Annu. Rev. Physiol.* **78,** 23–44
11. Tyni, T., Johnson, M., Eaton, S., Pourfarzam, M., Andrews, R., and Turnbull, D. M. (2002) Mitochondrial fatty acid β-oxidation in the retinal pigment epithelium. *Pediat. Res.* **52,** 595–600
12. Rodriguez de Turco, E. B., Gordon, W. C., Peyman, G. A., and Bazan, N. G. (1990) Preferential uptake and metabolism of docosahexaenoic acid in membrane phospholipids from rod and cone photoreceptor cells of human and monkey retinas. *J. Neurosci. Res.* **27,** 522–532
13. Gordon, W. C., Rodriguez de Turco, E. B., and Bazan, N. G. (1992) Retinal pigment epithelial cells play a central role in the conservation of docosahexaenoic acid by photoreceptor cells after shedding and phagocytosis. *Curr. Eye Res.* **11,** 73–83
14. Chen, H., and Anderson, R. E. (1993) Differential incorporation of docosahexaenoic and arachidonic acids in frog retinal pigment epithelium. *J. Lipid Res.* **34,** 1943–1955
15. Adijanto, J., Du, J., Moffat, C., Seifert, E. L., Hurle, J. B., and Philp, N. J. (2014) The retinal pigment epithelium utilizes fatty acids for ketogenesis. *J. Biol. Chem.* **289,** 20570–20582
16. Tyni, T., Paetau, A., Strauss, A. W., Middleton, B., and Kivelä, T. (2004) Mitochondrial fatty acid β-oxidation in the human eye and brain: implications for the retinopathy of long-chain 3-hydroxyacyl-CoA dehydrogenase deficiency. *Pediat. Res.* **56,** 744–750
17. Polinati, P. P., Ilmarinen, T., Trokovic, R., Hyotylainen, T., Otonkoski, T., Suomalainen, A., Skottman, H., and Tyni, T. (2015) Patient-specific induced pluripotent stem cell-derived RPE cells: understanding the pathogenesis of retinopathy in long-chain 3-hydroxyacyl-CoA dehydrogenase deficiency. *Invest. Ophthalmol. Vis. Sci.* **56,** 3371–3382
18. Kang, H. M., Ahn, S. H., Choi, P., Ko, Y. A., Han, S. H., Chinga, F., Park, A. S., Tao, J., Sharma, K., Pullman, J., Bottinger, E. P., Goldberg, I. J., and Susztak, K. (2015) Defective fatty acid oxidation in renal tubular epithelial cells has a key role in kidney fibrosis development. *Nat. Med.* **21,** 37–46
19. Cotter, D. G., Ercal, B., Huang, X., Leid, J. M., d'Avignon, D. A., Graham, M. J., Dietzen, D. J., Brunt, E. M., Patti, G. J., and Crawford, P. A. (2014) Ketogenesis prevents diet-induced fatty liver injury and hyperglycemia. *J. Clin. Invest.* **124,** 5175–5190
20. San Giovanni, J. P., and Chew, E. Y. (2005) The role of omega-3 long-chain polyunsaturated fatty acids in health and disease of the retina. *Prog. Retinal Eye Res.* **24,** 87–138
21. Bazan, N. G., and Rodriguez de Turco, E. B. (1994) Pharmacological manipulation of docosahexaenoic-phospholipid biosynthesis in photoreceptor cells: implications in retinal degeneration. *J. Ocular Pharmacol.* **10,** 591–604
22. van Kuijk, F. J., and Dratz, E. A. (1987) Detection of phospholipid peroxides in biological samples. *Free Radical Biol. Med.* **3,** 349–354
23. Damek-Poprawa, M., Diemer, T., Lopes, V. S., Lillo, C., Harper, D. C., Marks, M. S., Wu, Y., Sparrow, J. R., Rachel, R. A., Williams, D. S., and Boesze-Battaglia, K. (2009) Melanoregulin (MREG) modulates lysosome function in pigment epithelial cells. *J. Biol. Chem.* **284,** 10877–10889
24. Frost, L. S., Lopes, V. S., Stefano, F. P., Bragin, A., Williams, D. S., Mitchell, C. H., and Boesze-Battaglia, K. (2013) Loss of melanoregulin (MREG) enhances cathepsin-D secretion by the retinal pigment epithelium. *Vis. Neurosci.* **30,** 55–64
25. LaVail, M. M. (1976) Rod outer segment disc shedding in relation to cyclic lighting. *Exp. Eye Res.* **23,** 277–280
26. LaVail, M. M. (1980) Circadian nature of rod outer segment disc shedding in the rat. *Invest. Ophthalmol. Vis. Sci.* **19,** 407–411
27. Quazi, F., Lenevich, S., and Molday, R. S. (2012) ABCA4 is an *N*-retinylidene-phosphatidylethanolamine and phosphatidylethanolamine importer. *Nat. Commun.* **3,** 925
28. Weng, J., Mata, N. L., Azarian, S. M., Tzekov, R. T., Birch, D. G., and Travis, G. H. (1999) Insights into the function of Rim protein in photoreceptors and etiology of Stargardt's disease from the phenotype in abcr knockout mice. *Cell* **98,** 13–23
29. Singh, I., Lazo, O., and Kremser, K. (1993) Purification of peroxisomes and subcellular distribution of enzyme activities for activation and oxidation

of very-long-chain fatty acids in rat brain. *Biochim. Biophys. Acta* **1170,** 44–52
30. Du, J., Rountree, A., Cleghorn, W. M., Contreras, L., Lindsay, K. J., Sadilek, M., Gu, H., Djukovic, D., Raftery, D., Satrústegui, J., Kanow, M., Chan, L., Tsang, S. H., Sweet, I. R., and Hurley, J. B. (2016) Phototransduction influences metabolic flux and nucleotide metabolism in mouse retina. *J. Biol. Chem.* **291,** 4698–4710
31. Liu, J., Lu, W., Reigada, D., Nguyen, J., Laties, A. M., and Mitchell, C. H. (2008) Restoration of lysosomal pH in RPE cells from cultured human and ABCA4(−/−) mice: pharmacologic approaches and functional recovery. *Invest. Ophthalmol. Vis. Sci.* **49,** 772–780
32. Wang, W., Lee, S. J., Scott, P. A., Lu, X., Emery, D., Liu, Y., Ezashi, T., Roberts, M. R., Ross, J. W., Kaplan, H. J., and Dean, D. C. (2016) Two-step reactivation of dormant cones in retinitis pigmentosa. *Cell Reports* **15,** 372–385
33. Handa, J. T., Cano, M., Wang, L., Datta, S., and Liu, T. (2017) Lipids, oxidized lipids, oxidation-specific epitopes, and age-related macular degeneration. *Biochim. Biophys. Acta* **1862,** 430–440
34. Kurihara, T., Westenskow, P. D., Gantner, M. L., Usui, Y., Schultz, A., Bravo, S., Aguilar, E., Wittgrove, C., Friedlander, M., Paris, L. P., Chew, E., Siuzdak, G., and Friedlander, M. (2016) Hypoxia-induced metabolic stress in retinal pigment epithelial cells is sufficient to induce photoreceptor degeneration. *eLife* **5,** e14319
35. Jiang, M., Esteve-Rudd, J., Lopes, V. S., Diemer, T., Lillo, C., Rump, A., and Williams, D. S. (2015) Microtubule motors transport phagosomes in the RPE, and lack of KLC1 leads to AMD-like pathogenesis. *J. Cell Biol.* **210,** 595–611
36. O'Sullivan, T. N., Wu, X. S., Rachel, R. A., Huang, J. D., Swing, D. A., Matesic, L. E., Hammer, J. A., 3rd, Copeland, N. G., and Jenkins, N. A. (2004) dsu functions in a MYO5A-independent pathway to suppress the coat color of dilute mice. *Proc. Natl. Acad. Sci. U.S.A.* **101,** 16831–16836
37. Radu, R. A., Yuan, Q., Hu, J., Peng, J. H., Lloyd, M., Nusinowitz, S., Bok, D., and Travis, G. H. (2008) Accelerated accumulation of lipofuscin pigments in the RPE of a mouse model for ABCA4-mediated retinal dystrophies following vitamin A supplementation. *Invest. Ophthalmol. Vis. Sci.* **49,** 3821–3829
38. Adijanto, J., and Philp, N. J. (2014) Cultured primary human fetal retinal pigment epithelium (hfRPE) as a model for evaluating RPE metabolism. *Exp. Eye Res.* **126,** 77–84
39. Frost, L. S., Lopes, V. S., Bragin, A., Reyes-Reveles, J., Brancato, J., Cohen, A., Mitchell, C. H., Williams, D. S., and Boesze-Battaglia, K. (2015) The contribution of melanoregulin to microtubule-associated protein 1 light chain 3 (LC3) associated phagocytosis in retinal pigment epithelium. *Mol. Neurobiol.* **52,** 1135–1151
40. Ahmado, A., Carr, A. J., Vugler, A. A., Semo, M., Gias, C., Lawrence, J. M., Chen, L. L., Chen, F. K., Turowski, P., da Cruz, L., and Coffey, P. J. (2011) Induction of differentiation by pyruvate and DMEM in the human retinal pigment epithelium cell line ARPE-19. *Invest. Ophthalmol. Vis. Sci.* **52,** 7148–7159
41. De Rosa, M. C., Caputo, M., Zirpoli, H., Rescigno, T., Tarallo, R., Giurato, G., Weisz, A., Torino, G., and Tecce, M. F. (2015) Identification of genes selectively regulated in human hepatoma cells by treatment with dyslipidemic sera and PUFAs. *J. Cell. Physiol.* **230,** 2059–2066
42. Shenker, B. J., Ojcius, D. M., Walker, L. P., Zekavat, A., Scuron, M. D., and Boesze-Battaglia, K. (2015) *Aggregatibacter actinomycetemcomitans* cytolethal distending toxin activates the NLRP3 inflammasome in human macrophages, leading to the release of proinflammatory cytokines. *Infect. Immun.* **83,** 1487–1496
43. Boesze-Battaglia, K., Song, H., Sokolov, M., Lillo, C., Pankoski-Walker, L., Gretzula, C., Gallagher, B., Rachel, R. A., Jenkins, N. A., Copeland, N. G., Morris, F., Jacob, J., Yeagle, P., Williams, D. S., and Damek-Poprawa, M. (2007) The tetraspanin protein peripherin-2 forms a complex with melanoregulin, a putative membrane fusion regulator. *Biochemistry* **46,** 1256–1272
44. Boesze-Battaglia, K., Lamba, O. P., Napoli, A. A., Jr., Sinha, S., and Guo, Y. (1998) Fusion between retinal rod outer segment membranes and model membranes: a role for photoreceptor peripherin/rds. *Biochemistry* **37,** 9477–9487
45. Boesze-Battaglia, K., Fliesler, S. J., Li, J., Young, J. E., and Yeagle, P. L. (1992) Retinal and retinol promote membrane fusion. *Biochim. Biophys. Acta* **1111,** 256–262
46. Boesze-Battaglia, K., Hennessey, T., and Albert, A. D. (1989) Cholesterol heterogeneity in bovine rod outer segment disk membranes. *J. Biol. Chem.* **264,** 8151–8155
47. Wihlmark, U., Wrigstad, A., Roberg, K., Brunk, U. T., and Nilsson, S. E. (1996) Formation of lipofuscin in cultured retinal pigment epithelial cells exposed to pre-oxidized photoreceptor outer segments. *APMIS* **104,** 272–279
48. Nelson, C. P., Schunkert, H., Samani, N. J., and Erridge, C. (2015) Genetic analysis of leukocyte type-I interferon production and risk of coronary artery disease. *Arterioscler. Thromb. Vasc. Biol.* **35,** 1456–1462